Early Detection of Foot Ulcers through Asymmetry Analysis

Naima Kaabouch, Yi Chen, Wen-Chen Hu[a], Julie Anderson[b], Forrest Ames[c], and Rolf Paulson[d]
Electrical Engineering Department, University of North Dakota, ND 58202
[a]Computer Science department, , University of North Dakota, ND 58202
[b] College of Nursing, University of North Dakota, ND 58202
[c] Mechanical Engineering Department, University of North Dakota, ND 58202
[d] Altru Wound Clinic, Grand Forks, ND 58201

ABSTRACT

Foot ulcers affect millions of Americans annually. Areas that are likely to ulcerate have been associated with increased local skin temperatures due to inflammation and enzymatic autolysis of tissue. Conventional methods to assess skin, including inspection and palpation, may be valuable approaches, but usually they do not detect changes in skin integrity until an ulcer has already developed. Conversely, infrared imaging is a technology able to assess the integrity of the skin and its many layers, thus having the potential to index the cascade of physiological events in the prevention, assessment, and management of foot ulcers. In this paper, we propose a technique, asymmetry analysis, to automatically analyze the infrared images in order to detect inflammation. Preliminary results show that the proposed technique can be reliable and efficient to detect inflammation and, hence, predict potential ulceration.

Keywords: Foot Ulcers, Infrared Imaging, Asymmetry Analysis, Automatic Thresholding, Statistics

1. INTRODUCTION

Each year, millions of Americans are diagnosed with foot ulcers that present a risk of amputation. The populations most affected by ulcerations are diabetics and individuals with peripheral vascular disease. Patients with foot ulcers suffer from secondary conditions, including severe pain, immobility, increased infection risks, embarrassment and worry, and dramatic impact on quality of life. Furthermore, diabetes and its related complications have placed an economic burden on the U.S. healthcare system–in 2007, $174 billion, a 3% increase since 2002 [1]. About a fifth of these costs are directly related to diabetic foot ulcers and amputations. Therefore, it is imperative to develop new, more efficient techniques to address this important health concern.

One common mechanism in the development of foot ulceration involves a cumulative effect of unrecognized repetitive trauma at pressure points on the sole of the foot over the course of several days [2-4]. Areas that are likely to ulcerate have been associated with increased local skin temperatures due to inflammation and enzymatic autolysis of tissue [5-7]. Identifying areas of injury by the presence of inflammation would allow patients or healthcare providers to take early prospective, preventive action to decrease the inflammation before a wound or ulcer develops. This inflammation can mainly be characterized by five signs: redness, pain, swelling, loss of function, and heat. Some of these signs are difficult to assess. For examples, swelling and redness are difficult to objectively grade even among experienced clinicians. Additionally, patients may not notice the beginning of ulceration, because in the neuropathic extremity, pain and disturbance of function can be absent due to neuropathy, and, thus, these signs are poor indicators of inflammation [8]. However, temperature increase has been shown to be indicative of pending ulceration [9, 10].

In this paper, to detect inflammation, and hence predict foot ulcers infrared imaging is used to monitor the temperature distribution of the foot skin. Because skin-surface temperature of a healthy foot is affected by many factors--such as ambient and internal thermal conditions, age, sex, weight, etc.--one way to eliminate this variability is to compare the thermal skin distributions of two feet from the same subject. This comparison, asymmetry analysis, is combined with a thresholding technique to achieve higher accuracy an efficiency in the detection of inflammation and, hence, prediction of ulcers before they can develop.

Medical Imaging 2009: Biomedical Applications in Molecular, Structural, and Functional Imaging, edited by Xiaoping P. Hu, Anne V. Clough, Proc. of SPIE Vol. 7262, 72621L · © 2009 SPIE · CCC code: 1605-7422/09/$18 · doi: 10.1117/12.811676

2. METHODOLOGY

In this research work, the temperature of the skin is recorded during the natural cooling of the feet using a high resolution infrared camera, FLIR 500.

The resulting infrared images are then automatically analyzed using the following steps:

1. Automatic thresholding—to isolate the feet and remove as much noise as possible.
2. Geometric transformation—to adjust the left and the right feet so they are in the same positions in the image.
3. Asymmetry analysis—to subtract the intensity level of each pixel in the left foot from the intensity level of the symmetric pixel of the right foot to detect abnormal areas.
4. Features extraction—to enhance the effectiveness of the asymmetry analysis.

2.1 Automatic thresholding

In the proposed methodology, automatic thresholding of the thermal images is an important step to minimize the noise and decrease the detection of false inflammation. This step presents some challenges. First, some patients have feet that present areas with low temperatures, which are close to the temperatures of the images backgrounds. Second, the heat transfer from the legs and other body parts increases the temperature between the feet, resulting in highly non-uniform backgrounds. Figs. 1a, 1b, and 1c show three examples of infrared images that present non-uniform backgrounds mainly due to the transfer of heat from the legs and other body parts.

Therefore, to automatically analyze the feet, it is important to find a suitable thresholding technique for these types of infrared images. Thresholding techniques can be classified into several groups including

- Histogram shape-based methods
- Clustering-based methods
- Entropy-based methods
- Object attribute-based methods
- Genetic algorithms

Examples of these techniques have been addressed in a number of papers [11-21]. In this paper, we implemented one algorithm of each category and compared their performances. These algorithms are described below.

2.1.1 Histogram shape-based methods

This category of methods achieves image thresholding through the characteristics of the image histogram, such as peaks, valleys, and curvatures [12, 13]. One of the most referenced methods is Otsu's technique [12]. Otsu suggested minimizing the weighted sum of within-class variances of the foreground and background pixels to establish an optimum threshold given by

$$T_{opt} = \arg\max\left\{\frac{P(T)[1-P(T)][m_f(T)-m_b(T)]^2}{P(T)\sigma_f^2(T)+[1-P(T)]\sigma_b^2(T)}\right\} \quad (1)$$

Where m_b and m_f represent the mean values of the background and foreground, respectively, as functions of the thresholding level *T;* σ_b and σ_f represent the variance values of the background and foreground, respectively, as functions of the thresholding level *T.* $P(T)$ represents the cumulative probability as function of the thresholding level T. This probability is defined as

$$P(T) = \sum_{i=0}^{T} p(i) \tag{2}$$

2.1.2 Clustering-based methods

In clustering-based methods, the gray-level samples are clustered in two parts, background and foreground [14, 15]. One example of this category is Ridler's technique [15], which presented one of the first iterative schemes based on two-class Gaussian mixture models. The final thresholded image is obtained after many iterations. At each iteration *n*, a new threshold *Tn* is established using the average of the foreground and the background class means. In practice, iterations terminate when the difference $|Tn - Tn{+}1|$ becomes sufficiently small. The final optimal threshold level is given by

$$T_{opt} = \lim_{n\to\infty} \frac{m_f(T_n) + m_b(T_n)}{2} \tag{3}$$

Where

$$m_f(T_n) = \sum_{g=0}^{T_n} gp(g) \text{ and } m_b(T_n) = \sum_{g=T_n+1}^{G} gp(g) \tag{4}$$

Here, g represents an intensity level of the image;

$p(g)$ represents the probability mass function (PMF) of the image;

P_f and P_b represent the probability mass functions of the foreground and background, respectively;

m_f and m_b represent the mean of the foreground and background, respectively.

2.1.3 Entropy-based thresholding methods

Entropy-based methods use the entropy of the foreground and background regions as well as the cross-entropy between the original and binarized images [16, 17]. An example of such techniques was developed by Kapur et al. [16], in which the image's foreground and background are considered two different signal sources, so that when the sum of the two class entropies reaches its maximum, the image is said to be optimally thresholded. The optimal threshold is given by

$$T_{opt} = \arg\max[H_f(T) + H_b(T)] \tag{5}$$

Where

$$H_f(T) = -\sum_{g=0}^{T} \frac{p(g)}{P(T)} \log \frac{p(g)}{P(T)} \text{ and } H_b(T) = -\sum_{g=T+1}^{G} \frac{p(g)}{1-P(T)} \log \frac{p(g)}{1-P(T)} \tag{6}$$

g, $p(g)$, P_f, P_b, m_f, and m_b refer to the same variables as in section 2.1.2.

2.1.4 Object attribute-based thresholding methods

Object attribute-based methods search a measure of similarity between the gray-level and the binarized images, such as fuzzy shape similarity and edge coincidence [18, 19]. An example of such techniques is the moment preserving introduced by Tsai [18] who considers the gray-level image as the blurred version of an ideal binary image. The thresholding is established so that the first three gray-level moments match the first three moments of the binary image:

$$T_{opt} = \arg equal[m_1 = b_1(T), m_2 = b_2(T), m_3 = b_3(T)] \tag{7}$$

Where

$$m_k = \sum_{g=0}^{G} p(g) g^k \text{ and } b_k = P_f m_f^k + P_b m_b^k \tag{8}$$

Again, g, $p(g)$, P_f, P_b, m_f, and m_b refer to the same variables as in section 2.1.2.

2.1.5 Genetic algorithms-based thresholding techniques

Genetic algorithms are optimization algorithms based on biological mechanics of natural selection through a set of operations, such as chromosome, population size, cross rate, mutation rate, and maximum generation [20, 21].

The fitness is evaluated by

$$Fitness(x) = Num_f \cdot Num_b \cdot (M_f - M_b)^2 \tag{9}$$

Where Num_f and Num_b are the numbers of foreground and background pixels, respectively.

M_f, the mean intensity of foreground pixels, is given by

$$M_f = \frac{I_f}{Num_f} \tag{10}$$

Where I_f is the sum of intensities of foreground pixels.

M_b is the mean intensity of background pixels given by

$$M_b = \frac{I_b}{Num_b} \tag{11}$$

Where I_b is the sum of intensities of background pixels.

The best threshold is determined by the following equation:

$$Fitness(x^*) = \max\{Fitness(x)\} \tag{12}$$

Where x represents a population.

Major steps of the proposed genetic algorithm are summarized below:

1. Assign the length of chromosome, population size, cross rate, mutation rate, and maximum generation.
2. Initialize population of the first generation, with each individual being a random eight bits binary string, representing a specific intensity level.
3. Evaluate the fitness of the whole population.
4. Generate the next population by performing selection, crossover and mutation operations.

5. Go to step 3 if the desired number of generations is not reached.
6. Reduce the cross rate and mutation rate after half of the desired generation number is reached.
7. Segment the image using the optimal threshold level when the desired number of generation is reached.

2.2 Geometric transformation

The ultimate goal is to compare the thermal skin distributions of a healthy foot to the thermal distributions of a foot with abnormal areas. This comparison is achieved by subtracting the intensity levels of left foot from those of the right foot in the segmented image. However, the feet in the image are rarely in symmetric positions. Therefore, a geometric transformation is needed to adjust the positions of the feet. Assuming that the sizes of the feet are the same in the image, a simple translation and rotation around two feature points can achieve this purpose. The centroid and the furthest point from the centroid to the heel edge are chosen as references for the adjustment of each foot. Based on these two feature points, the relative position and angle differences between the two feet are calculated. Then, a rotation and a translation are performed to put each foot in the middle of the image with the characteristic line in the vertical direction. The geometric transformation procedure is described as follows:

1. Separate the original feet image into two images corresponding to the left foot and the right foot.
2. Identify the centroid and the furthest heel points of each foot.
3. Calculate the angle of the characteristic line with respect to the vertical direction.
4. Perform the translation and the rotation to adjust the feet in the middle of the image. First, each foot is shifted by moving the position of all pixels inside the foot to the center of the image. Then, the foot is rotated to make the characteristic line in the vertical direction.

2.3 Asymmetry analysis

In this step, the potential ulcerous areas are identified by analyzing the asymmetry between the adjusted feet images. Once the feet are adjusted in symmetric positions by using the geometric transformation algorithm, the left foot pixels intensities are subtracted from the corresponding right foot pixels intensities. If the difference exceeds a specific threshold the intensity is shown as abnormality in the image difference.

2.4 Features extraction

To quantify and to increase the effectiveness of the asymmetry analyses results, a last step consisting of features extraction is performed on the resulting image after thresholding, geometry transformation, and overlapping steps. The distribution of different intensities is quantified by calculating some high-order statistics for each foot, such as the mean, the variance, the skewness, the kurtosis, and the entropy. These parameters are, respectively, given by

$$\mu = \frac{1}{N}\sum_{i=1}^{N} p_i \tag{13}$$

$$\sigma = \frac{1}{N-1}\sum_{i=1}^{N} (p_i - \mu)^2 \tag{14}$$

$$Skewness = \frac{1}{N-1}\sum_{i=1}^{N} [\frac{(p_i - \mu)}{\sigma}]^3 \tag{15}$$

$$Kurtosis = \frac{1}{N-1}\sum_{i=1}^{N} [\frac{(p_i - \mu)}{\sigma}]^4 \tag{16}$$

$$Entropy = -\sum_{i=1}^{N} p_i \log p_i \tag{17}$$

Where p_i is the probability density of the ith bin in the histogram, and N is the total number of bins.

3. RESULTS

To assess the effectiveness of the developed technique, we accessed a large data set of infrared images corresponding to patients' feet with and without inflammation. Some examples of infrared images are illustrated in Figs. 1a – 1c. Figs. 1a and 1b show examples of infrared images of healthy feet, while Fig. 1c. shows another example of an infrared image in which the right foot contains a high temperature area, indicating the presence of inflammation. As can be seen from these images, the heat transfer from the legs in the infrared images generates a non-uniform background.

Examples of results after applying the five aforementioned thresholding techniques are shown in Figs. 2a - 2e. The most important criteria to assess these techniques are removing the noise resulting from the heat transfer around the feet and preserving their shapes. Based on these criteria, assessing a set of thresholded images indicates that the genetic algorithm provides better results than the other implemented techniques do.

However, no technique completely removed the noise between the feet. One of the solutions used to increase the efficiency of the thresholding techniques is separating the feet from the other parts of the body by using a light weight metallically painted shield. An example of the results is shown in Fig. 3. As observed, the quality of the thresholded image is greatly improved and the noise around the feet is completely removed. Fig. 4 represents the output images with adjusted feet after applying the geometric transformation to the thresholded image of Fig. 3. Fig. 5 shows the grayscale image representing the result of the asymmetry analysis. In this image, the white spot represents the location of the abnormal area.

Table 1 presents some examples of features extraction results corresponding to Fig. 3. From this table that compares the abnormal area in one foot with its corresponding normal area in the other foot, we observe that all statistics, except the entropy, are higher for a foot with inflammation and, thus, are effective in identifying abnormalities. The entropy remains the same and, thus, does not contribute to the detection of the asymmetry. Although the values of these features extraction results change, depending on the size and the temperature distributions of the inflammation, it can be stated that low and high order statistics, except the entropy, increase the effectiveness of asymmetry analysis for the detection of foot abnormalities.

Table 1. Examples of statistics for normal foot and foot with abnormalities.

	Normal	Abnormal
Mean	184	231
Variance	60	237
Skewness	0.26	0.4
Kurtosis	2.9	3.8
Entropy	0.19	0.19

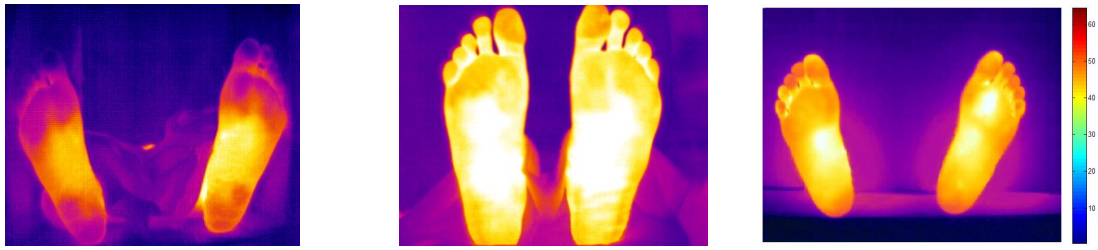

a b c

Figure 1: Example of infrared images corresponding to
a. healthy feet with cold temperatures areas;
b. healthy feet with non-uniform background due to the heat transfer around the feet.
c. foot with an abnormal area.

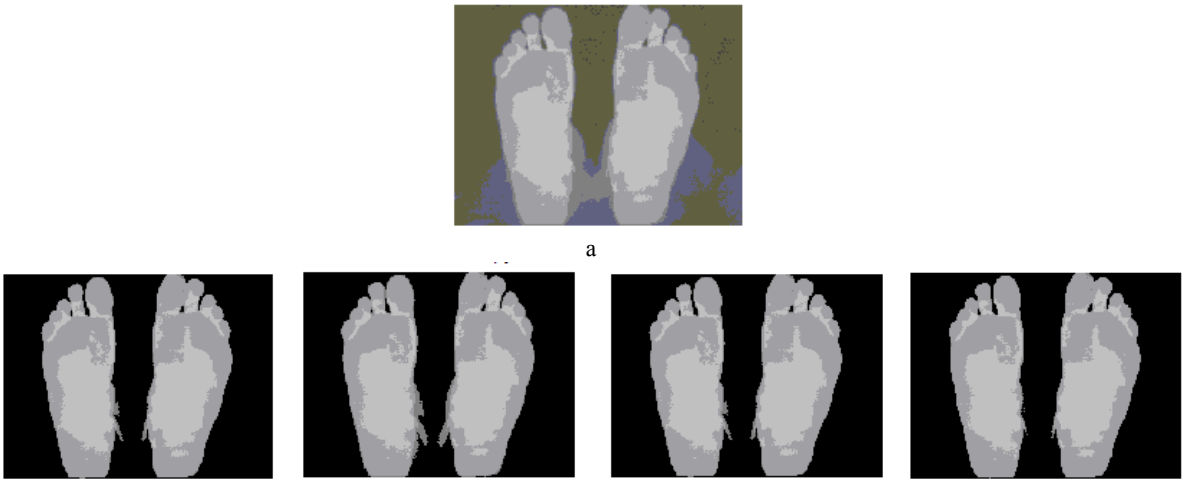

a

b c d e

Figure 2: Some results of the thresholding techniques:
a. grayscale image corresponding to the infrared image of Fig. 1b
b. output image after applying moment preserving method
c. output image after applying maximum entropy method
d. output image after applying Otsu's method
e. output image after applying the genetic algorithm.

Fig. 3: Output image after applying the genetic algorithm on Fig. 1c.

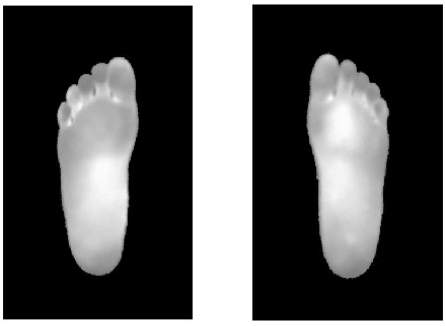

Fig. 4: Output images after applying the geometric transformation technique on Fig. 3.

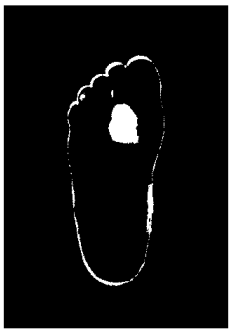

Fig. 5: Output image resulting from the asymmetry analysis of Fig. 4.

4. CONCLUSION

We developed an asymmetry analysis to investigate the thermal distributions of the feet in order to detect inflammation and, hence, predict foot ulcers. This technique is combined with features extraction (high order statistics) to increase the effectiveness of the proposed technique. The experimental results show that this technique is reliable to identify inflammation and, hence, predict potential ulceration. However, the developed technique assumes that the two feet are on the same plane in the image and have the same shape and size. Our objective, in the future, is to develop a technique that scans and compares symmetric pixels whatever the shape, the size, and the position of the feet.

ACKNOWLEDGMENT

This work was supported by the ND EPSCoR project through National Science Foundation grant # UND0012168.

REFERENCES

[1] http://www.diabetes.org/home.jsp

[2] Lavery L.A., Armstrong D.G., Vela S., and Fleishli J.G., "Practical criteria to screen patients at risk for diabetic foot ulceration," Arch. Int. Med., vol. 158, 157 – 162 (1998).

[3] Reiber G.E., Vileikyte L., Boyko E.J., del Aguila M., Smith D.G., Lavery L.A., and Boulton A.J., "Causal pathways for incident lower extremity ulcers in patients with diabetes from two settings," Diabetes Care, vol. 22, 157 – 162 (1999).

[4] Frykberg R.G., Lavery L.A., Pham H., Harvey C., Harkless L., and Veves A., " Role of neuropathy and high foot pressures in diabetic foot ulceration," Diabetes Care, vol. 21, 1714 – 1719 (1998).

[5] Armstrong D.G., Lavery L.A., Liswood P.J., Todd W.F., and Tredwell J., "Infrared dermal thermometry of the high-risk diabetic foot," Phys Ther, vol. 77, 169 – 177 (1997).

[6] Brand P.W., "The insensitive foot (including leprosy)", In Disorders of the Foot and Ankle. Jahss M., Ed. Philadelphia, Saunders, 2173 – 2175 (1991).

[7] Clark R.P., Goff M.R., Hughes J., and Klenerman L.,"Thermography and pedobarography in the assessment of tissue damage in neuropathic and atherosclerotic feet," Thermology, vol. 3, 15 – 20 (1988).

[8] Reiber G.E., Vileikyte L., Boyko E.J., del Aguila M., Smith D.G., Lavery L.A., and Boulton A.J., "Home monitoring of foot skin temperatures to prevent ulceration," Diabetes Care, vol. 27, 2642 – 2647 (2004).

[9] Schubert V, Fagrell B., "Evaluation of the dynamic cutaneous post ischaemichyperaemia and thermal response in elderly subjects and in an area at risk for pressure sores," Clin Physiol, vol. 11, 69 – 182 (1991).

[10] Armstrong D.G. and Lavery L.A., "Predicting neuropathic ulceration with dermal thermography," J. Am. Podiatr. Med. Assoc., vol. 87, 336 – 337 (1997).

[11] M. Sezgin and B. Sankur "Survey over image thresholding techniques and quantitative performance evaluatio," J. of Electronique Imaging, 13(1), 146 – 165 (2004).

[12] N. Otsu, ''A threshold selection method from gray level histograms,'' IEEE Trans. Syst. Man Cybern. **SMC-9**, 62 – 66 (1979).

[13] M. J. Carlotto, ‘‘Histogram analysis using a scale-space approach,’’ IEEE Trans. Pattern Anal. Mach. Intell. PAMI-9, 121 – 129, (1997).
[14] C. V. Jawahar, P. K. Biswas, and A. K. Ray, ‘‘Investigations on fuzzy thresholding based on fuzzy clustering,’’ Pattern Recogn. 30-10, 1605 – 1613 (1997).
[15] T. W. Ridler and S. Calvard, ‘‘Picture thresholding using an iterative selection method,’’ IEEE Trans. Syst. Man Cybern. SMC-8, 630 – 632 (1978).
[16] J. N. Kapur, P. K. Sahoo, and A. K. C. Wong, ‘‘A new method for gray-level picture thresholding using the entropy of the histogram,’’ Graph. Models Image Process. 29, 273 – 285 (1985).
[17] C. H. Li and P. K. S. Tam, ‘‘An iterative algorithm for minimum cross-entropy thresholding,’’ Pattern Recogn. Lett. 19, 771 – 776 (1998).
[18] W. H. Tsai, ‘‘Moment-preserving thresholding: A new approach,’’ Graph. Models Image Process. 19, 377 – 393 (1985).
[19] X. Fernandez, ‘‘Implicit model oriented optimal thresholding using Kolmogorov-Smirnov similarity measure,’’ ICPR’2000: Intl. Conf. Patt. Recog., 466 – 469 (2000).
[20] Goldber D.E., “Genetic algorithms in search, optimization and machine learning,” Addison-Wesley, (1989).
[21] Kaabouch N., Chen Y., Anderson J., Ames F., and Paulson R., “Asymmetry analysis based on genetic algorithms for the prediction of foot ulcers,” SPIE Electronic Imaging Proceedings, (2009).